Int. J. Electrochem. Sci., 15 **(2020)** 10922 – 10935, doi: 10.20964/2020.11.02

International Journal of ELECTROCHEMICAL SCIENCE
www.electrochemsci.org

Discharge and Corrosion Behaviors of Mg-Li and Mg-Li-La Alloys as Anodes for Seawater Battery

Juxin Yu[1,2], *Yanzhuo Lv*[1,*], *Tigang Duan*[2,*], *Fei Meng*[1], *Qing Cheng*[1], *Yan Xu*[4], *Kaiwen Zhou*[1], *Lili Xue*[1], *Zhe Leng*[3,*"].

[1] Key Laboratory of Superlight Material and Surface Technology of Ministry of Education, the College of Material Science and Chemical Engineering, Harbin Engineering University, Harbin 150001, P.R. China;
[2] State Key Laboratory for Marine Corrosion and Protection, Luoyang Ship Material Research Institute, Qingdao 266237, P.R. China;
[3] Innovation and Application Institute, Zhejiang Ocean University, Zhoushan 316022, P.R. China;
[4] Engineering Training Center, Harbin Engineering University, Harbin 150001, China.
[*]E-mail: lvyanzhuo@hrbeu.edu.cn, duantigang@sunrui.net, lengzhe@zjou.edu.cn

Received: 16 June 2020 / *Accepted:* 12 August 2020 / *Published:* 30 September 2020

The electrochemical performance of Mg-8Li-0.5La and Mg-8Li-1La alloy as anodes for seawater battery were investigated by electrochemical techniques. Scanning electron microscopy (SEM) was used to characterize the microstructures and the corroded surfaces of the above anodes. X-ray diffraction (XRD) was used to analyze the composition and the crystalline pattern of the discharging products. Results show that Mg-8Li-1La anode has the higher electrochemical activity and the better corrosion resistance. Potentiodynamic polarization shows that the corrosion potentials of Mg-8Li-1La alloy anode and Mg-8Li-0.5La alloy anode are -1.64 V and -1.67 V (vs. SCE), respectively, which are more active than the Mg-8Li alloy anode(-1.57 V vs. SCE). The current densities for anodes at the discharge voltage of -1.0 V increase with the following order: Mg-8Li (31 $mA \cdot cm^{-2}$) < Mg-8Li-0.5La (35 $mA \cdot cm^{-2}$) < Mg-8Li-1La (42 $mA \cdot cm^{-2}$). The Mg-8Li-1La alloy anode provides a more negative voltage than Mg-8Li-0.5La alloy anode and Mg-8Li alloy anode during the galvanostatic discharge test. Therefore, the content of La in alloys obviously affects the electrochemical performance of alloys.

Keywords: Mg-8Li-0.5La; Mg-8Li-1La; Alloy anode; Discharge behaviors; Electrochemical performance; Sodium chloride solution

1. INTRODUCTION

Unlike magnesium-air semi-fuel cells and other conventional land-based fuel cells that rely on air to supply oxygen, magnesium-hydrogen peroxide semi-fuel cells carrying liquid hydrogen peroxide

as oxidants can operate in an anaerobic environment such as underwater and space. Thus, magnesium-hydrogen peroxide semi fuel cells have been developed as the power sources for low rate, long endurance unmanned underwater vehicles (UUV) [1-3]. Magnesium-hydrogen peroxide half-fuel battery possesses the advantages of safe, low cost, high energy density, stable discharge capacity, short mechanical recharging time, long shelf life, simple structure, friendly environment, strong reliability, high discharge in seawater electrolyte [4-8]. In addition, the most outstanding feature of this battery is a combination of the highly-discharging active alloy anode and the open-structured hydrogen peroxide cathode. During the battery discharges, the electrolyte promotes the ionization of alloy anode to provide electrons for power generation [9].

During the cell discharges, magnesium alloys are oxidized and hydrogen peroxide is reduced. The electrode reaction processes are shown as below [10]:

$$Mg \rightarrow Mg^{2+} + 2e^{-} \qquad (E^{\theta}=2.37\ V) \qquad (1)$$

$$H_2O_2 + 2H^{+} + 2e^{-} \rightarrow 2H_2O \qquad (E^{\theta}=1.77\ V) \qquad (2)$$

The cell reaction is shown as below:

$$Mg + H_2O \rightarrow Mg(OH)_2 + H_2\uparrow \qquad (E^{\theta}=4.14\ V) \qquad (3)$$

Magnesium is an exceptional choice of anode because of its negative standard electrode potential of -2.37 V (vs. SHE) and its high Faradic capacity of 2.2 $Ah \cdot g^{-1}$ [11-14]. However, the magnesium anode actually shows a lower negative potential, mainly due to the passivation film covering on the magnesium surface, resulting in a delay to reach a steady state and a decrease in the discharging rate. In addition, the magnesium anode exhibits a self-discharge phenomenon accompanying with the self-corrosion and the hydrogen evolution reaction during the discharge process. One way to solve the above problems is to introduce other elements into the magnesium alloy. Lithium located in the first main group of the periodic table is the most active metal among the known elements (including the radioactive elements) and has the most negative electrode potential. The Mg-Li alloy anode has a high discharge activity and a high energy density, and thus it attracts more attention as the potential substituted electrode material. Currently, the alloying elements, such as aluminum, cesium, yttrium, rare earth (RE) and so on, are introduced to improve the electrochemical behaviors of Mg-Li binary alloys. Cao [12] studied the electrochemical performances of Mg-Li, Mg-Li-Al, and Mg-Li-Al-Ce alloy anodes. Their electrochemical behaviors in 0.7 $mol \cdot L^{-1}$ NaCl solutions were investigated. Discharge activities and utilization efficiencies of these alloys increase in the order: Mg-Li < Mg-Li-Al < Mg-Li-Al-Ce. These three Mg-Li based alloys demonstrate the higher potentiostatic discharge current in NaCl solution than AZ31 alloys. Song [15] studied the corrosion characterization of Mg-8Li alloy in NaCl solution. The electrochemical results indicate that the corrosion resistance of Mg-8Li alloy in 0.1 $mol \cdot L^{-1}$ NaCl solution gradually deteriorates with the immersion time increases. Ma [16] studied the electrochemical characterization of Mg-Li-Al-Ce alloy. They found that the self-corrosion rates of these alloys are in the order: Mg-Li-Al-Ce < Mg < AZ31. It has been observed that Mg-Li-Al-Ce anode offers higher operating voltage, anodic efficiency and energy than Mg and AZ31. In addition, SEM and EIS results display that the discharge products of Mg-Li-Al-Ce alloy are loosely adhered to the alloy surface, and thus Mg-Li-Al-Ce alloy can keep the high discharge activity during discharging. Our group [17] reported the electrochemical behaviors of Mg-Li-Al-Ce and Mg-Li-Al-Ce-Y alloy anodes in 0.7 $mol \cdot L^{-1}$ NaCl solution. It was found that Y can change the alloy structure or assist the formation of an easy-peel off layer on the alloy surface. Our group

[18] also demonstrated that the Mg-8Li-0.5Y electrode has a higher discharge activity and a less corrosion resistance than the Mg-8Li-1Y electrode. The content of Y in the alloys obviously affected the alloy performances and the Y content of 0.5 wt.% is better than 1.0 wt.%. Furthermore, our group [19] also investigated the electrochemical behaviors of Mg-5Li-3Al-1La and Mg-8Li-3Al-1La alloys in sodium chloride solution. The results show that the Mg-8Li-3Al-1La alloy displays a better salt compatibility than the Mg-5Li-3Al-1La alloy, and the electrolyte can easily permeate the electrode.

For recent years, the application of rare earth elements in alloys has attracted extensive attention, but there have been few reports on the effect mechanism of rare earth element doping on the performance of alloys. Therefore, in this work, the rare earth element La was taken as the research object and the effects of La content were investigated on the electrochemical behaviors of the bimetallic Mg-8Li alloys anode. The Mg-8Li, Mg-8Li-0.5La and Mg-8Li-1La alloys were prepared, and their electrochemical behaviors in 0.7 $mol \cdot L^{-1}$ NaCl solution were studied.

2. EXPERIMENTAL

2.1 Preparation of the Mg-Li-based alloys

Table 1. Nominal compositions of the alloys (wt.%).

Alloys	Mg	Li	La
Mg-8Li	92	8	-
Mg-8Li-0.5La	91.5	8	0.5
Mg-8Li-1La	91	8	1

The Mg-Li and Mg-Li-La alloys were prepared from ingots of pure magnesium (99.99%), pure lithium (99.99%), and Mg-La alloy containing 20.02 wt.% La using a vacuum induction melting furnace under an ultrahigh purity argon. Mg-8Li, Mg-8Li-0.5La and Mg-8Li-1La alloys were prepared using metal with 99.99% purity in order to avoid interference by other elements. The ingredients of alloys were first put into an induction furnace, then vacuumed to 1.0×10^{-2} Pa, and heated to 700 ℃ to melt the metal components. AC power was applied throughout the process under the flowing argon atmosphere. Finally, the obtained molten alloy was poured into a stainless steel mold and cooled in an argon atmosphere for 24 h to the ambient temperature. Nominal compositions of the alloys are given in Table 1.

2.2 Electrochemical measurements

The prepared alloys were cut into 15 mm×15 mm×2.5 mm, one side of the sample was used as

the test surface. The test surface was successively polished with 400 #, 1200 # and 2000 # metallographic emery papers until a mirror-like smooth surface condition, and washed with deoxygenated ultrapure water (Milli-Q), degreased with acetone and rinsed with deoxygenated ultrapure water again, dried with hair dryer lastly, and then immediately installed into the electrochemical test instrument.

In the electrochemical measurements, a specifically designed home-made three-electrode electrochemical cell was used, the saturated calomel electrode (SCE) was used as the reference electrode, the platinum foil and magnesium alloys were used as the counter electrode and the working electrode, respectively. The electrochemical experiments were performed with a CHI660D electrochemical workstation in 0.7 $mol \cdot L^{-1}$ NaCl solution.

After the magnesium alloys were immersed in the 0.7 $mol \cdot L^{-1}$ sodium chloride solution for 5 minutes to obtain a stable open circuit potential (OCP), the polarization curves of magnesium alloys were measured by the potentiodynamic polarization scanning method. The constant current discharge method was used to obtain the potential-time curve of the magnesium alloy electrode, and the constant potential discharge method was used to obtain the current-time curve. Additional anode current densities of 10 $mA \cdot cm^{-2}$, 30 $mA \cdot cm^{-2}$, 40 $mA \cdot cm^{-2}$, and 60 $mA \cdot cm^{-2}$ were used for 600 s in the potential-time discharging process, and the anode potential of -1.0 V was applied in the current-time discharging process, respectively. The electrochemical impedance spectra (EIS) were carried out at the OCP after the samples were immersed in the electrolyte for 5 minutes. The scan frequency ranged from 100 kHz to 0.1 Hz and the perturbation amplitude was 5 mV. The measured EIS was then fitted with Zview software.

2.3 Microstructure characterization

The microstructure and the morphology of the corrosion surface of each sample were determined by scanning electron microscope (SEM, JSM-6480, Japan). In addition, X-ray diffractometer (XRD, D8ADVANCE, Germany) was employed to investigate the crystalline patterns of alloy samples, and Cu Kα radiation was used to identify the products of three alloys with the scan range of 2θ from 10° to 80° and the scan speed of 4° min^{-1}.

3. RESULTS AND DISCUSSION

3.1 Potentiodynamic polarization

The potentiodynamic polarization curve represents the connection between the logarithm of the current and the potential. The corrosion current density and the corrosion potential of alloy can be determined by the curve [20, 21]. Figure 1 shows the potentiodynamic polarization curves of Mg-8Li-0.5La, Mg-8Li-1La and Mg-8Li electrodes measured in 0.7 $mol \cdot L^{-1}$ NaCl solution, and Table 2 shows the corrosion parameters of magnesium alloy electrodes measured in 0.7 $mol \cdot L^{-1}$ NaCl solution.

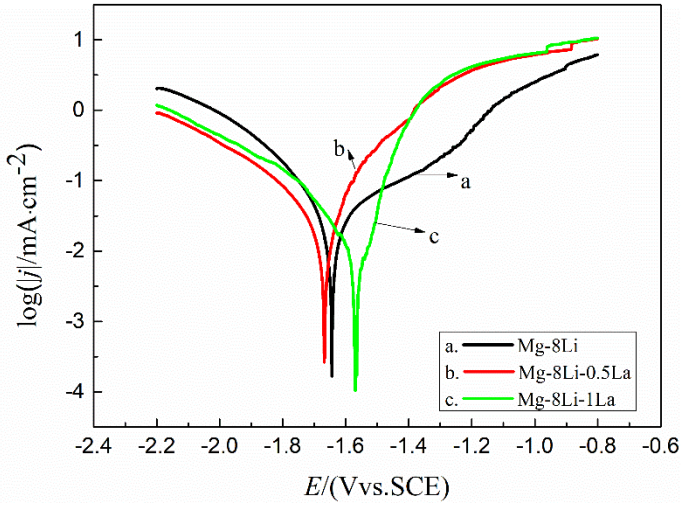

Figure 1. Potentiodynamic polarization curves of Mg-8Li (a), Mg-8Li-0.5La (b) and Mg-8Li-1La (c) electrodes measured in 0.7 mol·L^{-1} NaCl solution with a scan rate of 5 mV·s^{-1}.

Table 2. Electrochemical data of alloy electrodes in 0.7 mol·L^{-1} NaCl solution.

Alloy electrodes	Corrosion potential /V(vs. SCE)	Corrosion current density /μA·cm^{-2}	Open circuit potential /V(vs. SCE)
Mg-8Li	-1.57	14.83±2.1	-1.71
Mg-8Li-0.5La	-1.67	17.43±4.6	-1.75
Mg-8Li-1La	-1.64	20.47±4.8	-1.75

Seen from Table 2, the corrosion potential of Mg-8Li-0.5La electrode is -1.67 V, which is 100 mV more negative than that of Mg-8Li electrode. The corrosion potential of Mg-8Li-1La electrode is -1.64 V, which is 70 mV more negative than that of Mg-8Li electrode. Obviously, it also can be seen from Table 1 that the Mg-8Li electrode has a relatively positive corrosion potential and a small corrosion current density, indicating that the activity of Mg-8Li electrode is not as active as Mg-8Li-0.5La electrode and Mg-8Li-1La electrode. Thus, from the view of thermodynamics, adding La element may increase the electrochemical activity of Mg-8Li alloy electrode. For alloy electrodes, the cathodic side of the Mg-8Li curve is the highest, indicating that the hydrogen evolution rate of Mg-8Li electrode is the largest. And the anodic side of the Mg-8Li-1La and the Mg-8Li-0.5La curves is higher than that of the Mg-8Li curve, which indicates the activity of the former two electrodes is higher than that of the latter electrode. The content of La has a significant effect on the potentiodynamic polarization curves. The reason for these behaviors may be related to the chemical composition and the structure of the magnesium alloy. The addition of La do not only refines the grains, but also helps to remove impurities during the melting of magnesium alloy [19]. Thus, adding of La element can improve the performances of Mg-8Li electrode.

3.2 The self-corrosion rate and the self-discharge rate

The purpose to test the self-corrosion rate and the self-discharge rate is to examine the active utilization of magnesium-lithium alloy as the anode material of battery.

Table 3. The self-corrosion rate and the self-discharge rate of electrodes in 0.7 mol·L^{-1} NaCl solution.

Alloy electrodes	Initial weight /g	Final weight /g	Lost weight/ g	*n*	*Ma*	Self-corrosion rate for 24h *v*/(mg·cm^{-2}·min^{-1})	Self-discharge rate for 24h *j*/（mA·cm^{-2}）
Mg-8Li	1.5637	1.598	0.0039	1.7665	20.2551	0.0054	0.7654
Mg-Li-0.5La	1.5566	1.5529	0.0037	1.7665	20.3250	0.0051	0.7088
Mg-8LI-1La	1.5706	1.5670	0.0036	1.7664	20.3955	0.0050	0.6942

The self-corrosion rate (v) and the self-discharge rate (j) of alloy electrodes were calculated by the Eqs. (4-5). The results are shown in Table 3.

$$v = (m_0 - m_t)/(s \times t) \tag{4}$$

$$j = \frac{(m_0 - m_t) \times nF}{M_a \times t \times S} \tag{5}$$

As shown in Table 3, the corrosion rate of Mg-8Li alloy is 0.0054 mg·cm^{-2}·min^{-1}, which is 8.0% higher than that of Mg-8Li-1La alloy. Moreover, the corrosion rate of Mg-8Li-0.5La alloy is 0.0051 mg·cm^{-2}·min^{-1}, which is 2.0% higher than that of Mg-8Li-1La alloy. It is obvious that the corrosion rate of Mg-8Li-1La alloy is the lowest. In addition, the self-discharge rates of Mg-8Li, Mg-8Li-0.5La and Mg-8Li-1La alloys are 0.7654 mA·cm^{-2}, 0.7088 mA·cm^{-2}, and 0.6942 mA·cm^{-2}, respectively, and the Mg-8Li-1La alloy also has the lowest value. The self-corrosion rates and the self-discharge rates of Mg-8Li-0.5La alloy and Mg-8Li-1La alloy are lower than that of Mg-8Li alloy, indicating that the alloying element of La may change the crystal structure of Mg-8Li alloy and can enhance the protective property of the $Mg(OH)_2$ film on the alloy [22, 23]. Obviously, the self-corrosion rate is consistent with the self-discharge rate, and the Mg-8Li-1La alloy has the smallest value among three alloys. Thus, it indicates that if these electrodes are assembled into a metal half-fuel cell placed under natural conditions, the Mg-8Li-1La electrode is more resistant to corrosion and self-discharge than the other two electrodes.

3.3 The constant potential oxidation curves

The constant potential oxidation curve is also called as the timing current curve. It sets the working potential to a fixed value to record the variation of working current with the time. By comparing the magnitude of the anodization current density, the electrooxidation activity of the electrode can be

obtained. Further, it is possible to judge the stability performance of the electrode, and the more stable the electrode performance, the more efficiently the fuel cell can be operated. The current-time curves of Mg-8Li, Mg-8Li-0.5La and Mg-8Li-1La alloy electrodes at -1.0 V were measured and shown in Figure 2.

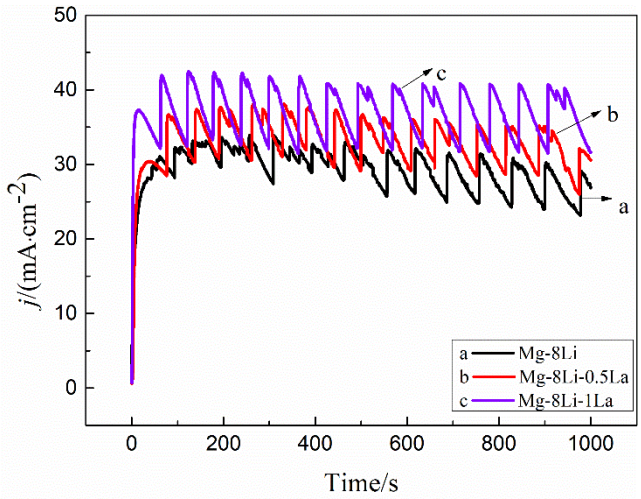

Figure 2. Potentiostatic current-time curves at -1.0 V in 0.7 mol·L^{-1} NaCl solution.

As seen from Figure 2, each discharge curve has a jagged appearance in different degrees. This may be due to the change of the effective electrode surface caused by the accumulation of products on the surface. The continuous formation and accumulation of oxides on the electrode surface during discharging has hindered the sufficient contact of the electrode surface with the electrolyte. The effective discharge area of the electrode is reduced, resulting in a decrease of the anodic current density. Discharge products gradually accumulate to a certain extent and are peeled off from the electrode surface, then the effective discharge area returns to its original size and the anodic oxidation current density increases [13]. Therefore, this results in a jagged curve. In addition, it can be seen that it takes longer time for current to reach the steady value for Mg-8Li electrode than the other two samples at the initial discharge period. The Mg-8Li-1La electrode exhibits a shortest transition time that the current reaches the stable value and exhibits a smaller "lag effect". The overall discharge currents for these alloy electrodes exhibit a little decrease within the test period at -1.0 V, and the Mg-8Li-1La electrode possesses the highest current density (about 42 mA·cm^{-2}) within the measuring period. The discharge current density of Mg-8Li-0.5La electrode is around 4 mA·cm^{-2}, which is higher than that of Mg-8Li electrode under the same discharge potential. The activity increases in the following order: Mg-8Li < Mg-8Li-0.5La < Mg-8Li-1La. The Mg-Li-La alloy electrode show better discharge performance than the Mg-Li alloy electrode under the same experimental condition. This result is closely related to the properties of the La element itself, one of which is that the La element is soft, malleable and paramagnetic. Since the outer electronic arrangement of La element is $5d^16s^2$, it has a strong metal activity. In addition, the size and the electronegativity of Mg atom and La atom are similar, so La has a large solubility in Mg, and thus both elements exhibit high activity at the same time. These reasons may be another factor for improving the activity of the alloy electrode. It can be concluded from the potentiostatic current-time curves that the

incorporation of La element into the binary Mg-8Li alloy can activate the alloy and improve its discharging current.

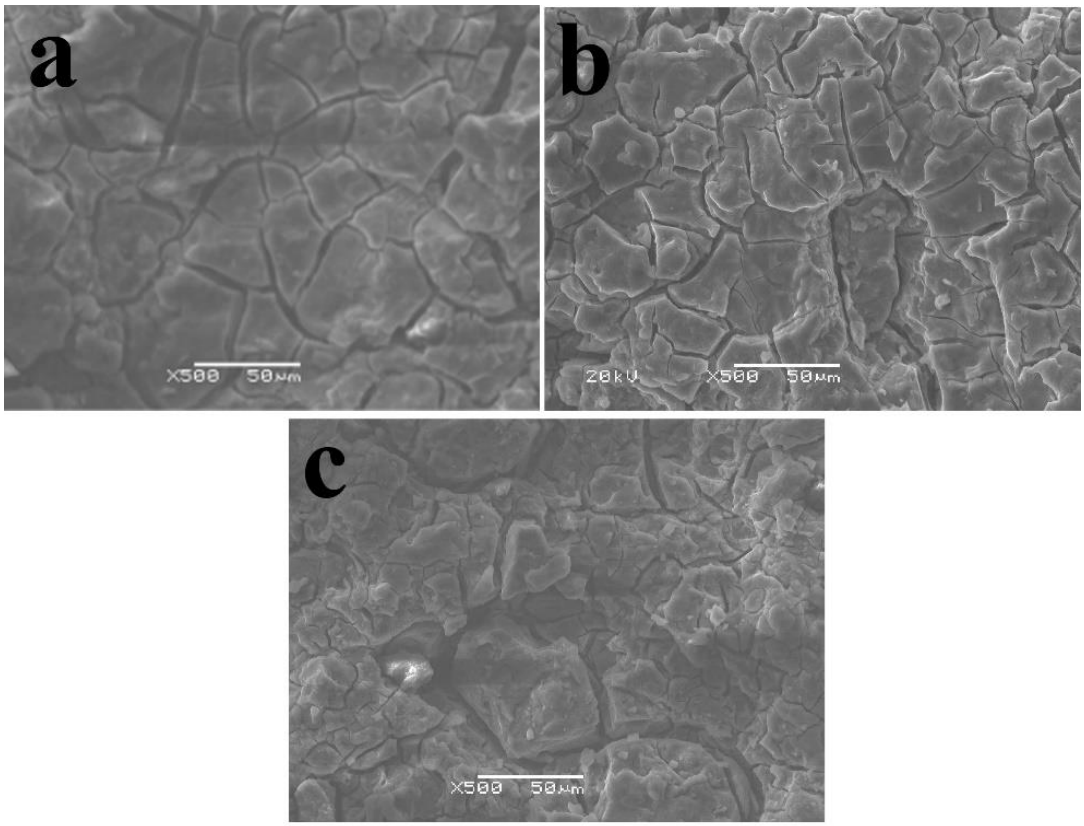

Figure 3. SEM micrographs of alloys after discharged at -1.0 V each for 1000 s, (a) Mg-8Li, (b) Mg-8Li-0.5La, (c) Mg-8Li-1La.

The SEM images were taken after the samples were consecutively discharged at -1.0 V each for 1000 s. Figures 3(a-c) show the SEM micrographs of Mg-8Li (a), Mg-8Li-0.5La (b) and Mg-8Li-1La (c) alloys, respectively.

Obviously, the surface morphologies of three samples vary under the same conditions. Figure 3(a) indicates that the oxidation products of Mg-8Li electrode is relatively smooth and large, so the contact between the active electrode surface and the electrolyte is hindered by large microblocks. On the contrary, most of surfaces of Mg-8Li-0.5La and Mg-8Li-1La alloys are covered by relatively loosely packed aggregates, and deep cracks in Figures 3(b) and (c), which allow the electrolyte to penetrate easily. The product gills formed by the oxidation products of the Mg-8Li-0.5La alloy are shallower than that of Mg-8Li-1La alloy and the range of crack is smaller, indicating that the Mg-8Li-1La alloy electrode has a sufficient reaction with the electrolyte, which in turn improves the electrochemical activity of the electrode. The SEM results suggest that the alloying element of La weakens the formation of dense passive film on the surface of the electrode and may facilitate the film peeling off from the alloy surface. This is because the discharge product of Mg-8Li-1La electrode is not easily adhered, so it is easy to fall off from the electrode surface. This facilitates sufficient contact between the electrode and the electrolyte to maintain a large effective discharge area. In summary, this is one of the reasons why

the Mg-8Li-1La alloy anode has high discharge activity.

3.4 XRD analysis

In order to study the composition of discharge products of Mg-8Li, Mg-8Li-0.5La and Mg-8Li-1La alloy electrodes, X-ray diffraction tests were carried out, and the test results are shown in the Figure 4.

These products are obtained by filtering the electrolyte after each sample is discharged at -1.0 V for 3 h. It can be seen that the main component of discharge products is $Mg(OH)_2$, and three strong diffraction peaks of $Mg(OH)_2$ are observed, peaking at around 2θ = 18.1°-19.1°, 37.8°-38.1° and 50.7°-51.0°, respectively. In addition, the weak peak of $Mg_2(OH)_3Cl{\cdot}4H_2O$ is found in XRD patterns, peaking at around 2θ = 10.7°-11.2°. Moreover, some peaks of NaCl also exist in all the XRD patterns, and the discharge products of Mg-8Li-1La alloy display significantly stronger peak intensity of NaCl than that of the other two samples. It can be considered that the Mg-8Li-1La exhibits better compatibility with the salt. NaCl is well to promote the dissolution of insoluble reaction products (i.e., $Mg(OH)_2$) and the peeling of the deactivation products. Thus, La can be deemed to activate the Mg-8Li alloy electrode. Additionally, the reaction products of La can not be identified owing to the low content in magnesium alloy.

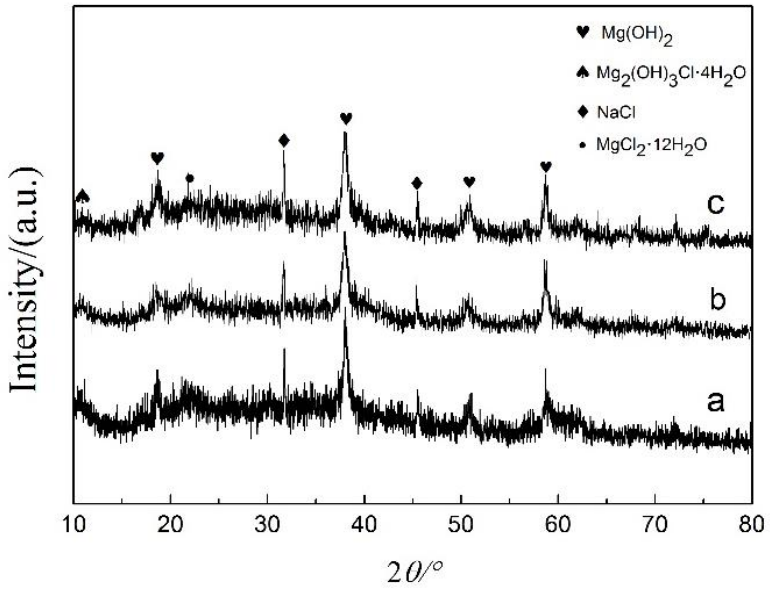

Figure 4. X-ray diffraction patterns of the alloys, (a) Mg-8Li, (b) Mg-8Li-0.5La, (c) Mg-8Li-1La.

3.5 Constant current oxidation curve

The constant current oxidation curve is also called as the timing-voltage curve, that is, the variation of the working voltage with the time is recorded with the working current being a constant value. Therefore, the electrode is kept at some different current densities and the change in oxidation

voltages are tested for a long time to investigate whether the electrode performance is stable. The voltage-time curves of Mg-8Li, Mg-8Li-0.5La, and Mg-8Li-1La alloy electrodes in 0.7 mol·L^{-1} NaCl solution are presented in Figure 5. The average discharge voltages of Mg-8Li, Mg-8Li-0.5La, and Mg-8Li-1La electrodes at different current densities for 600 s are listed in Table 4.

Table 4. Average discharge voltages of Mg-8Li, Mg-8Li-0.5La, Mg-8Li-1La alloy electrodes at different current densities for 600 s in 0.7 mol·L^{-1} NaCl solution.

Alloy electrodes	Average discharge voltage /V			
	10 mA·cm^{-2}	20 mA·cm^{-2}	30 mA·cm^{-2}	40 mA·cm^{-2}
Mg-8Li	-1.51	-1.32	-1.21	-0.98
Mg-8Li-0.5La	-1.61	-1.44	-1.27	-1.07
Mg-8Li-1La	-1.69	-1.48	-1.29	-1.11

In this work, a small current density of 10 mA·cm^{-2} is assigned to investigate the discharge behaviors of the magnesium alloy anodes used for long-term low-power applications. As can be seen from Figure 5, the discharge voltage of electrode increases with the increase of current density. It is because that when the current density increases, the reaction rate of electrode will increase, and the polarization degree of electrode will increase. The greater the polarization overpotential, the more positive the potential will be. According to Figure 5, the curve of Mg-8Li-1La electrode at 10 mA·cm^{-2} is relatively stable, indicating that the addition of La element refines the grains of alloy and improve the uniformity of the reaction, so that the discharge product is easily detached from the electrode surface [24, 25]. From Table 4, Mg-8Li-0.5La and Mg-8Li-1La electrodes show more negative voltages than Mg-8Li electrode at the same current density. Thus, lanthanum does not only accelerate the activation process of the Mg-8Li alloy in the initial discharge but also enhances its discharge activity in the steady-state.

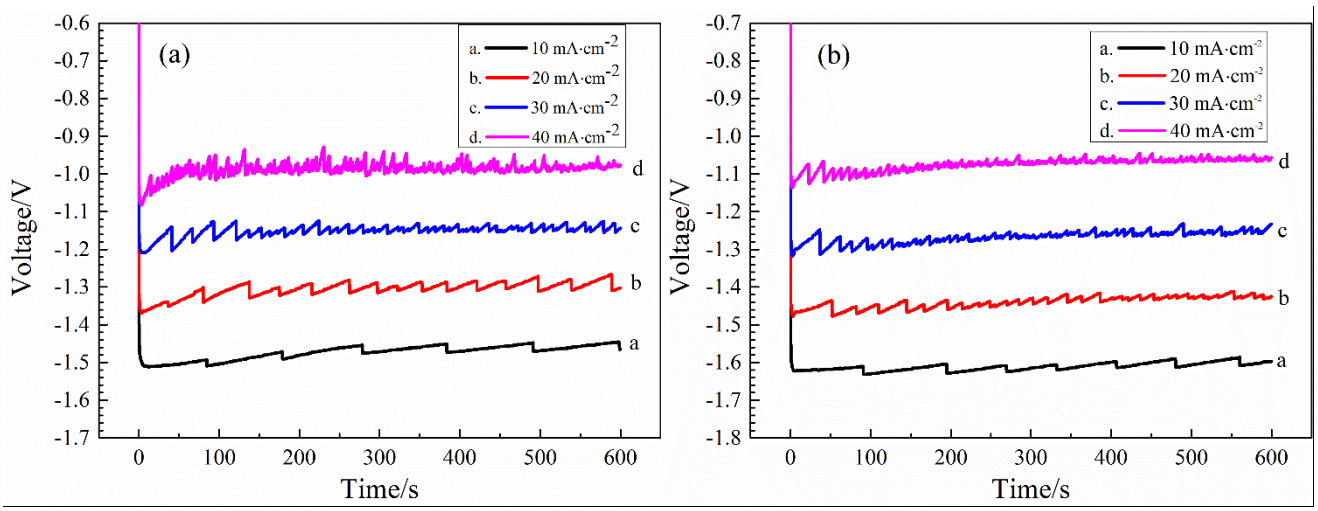

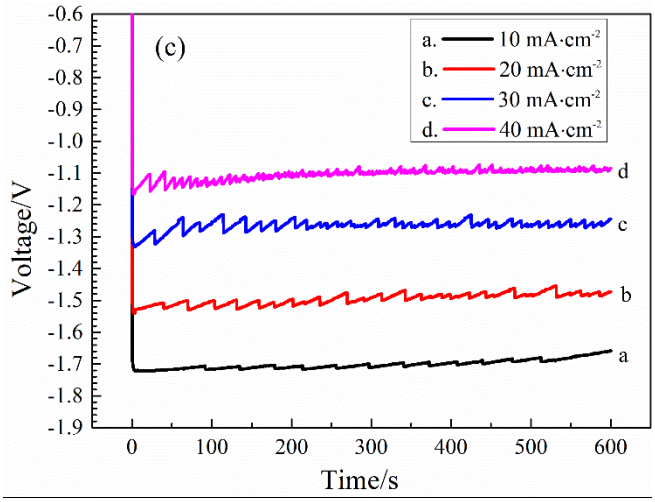

Figure 5. Galvanostatic voltage-time curves of alloy electrodes in 0.7 mol·L^{-1} NaCl solution, (a)Mg-8Li, (b)Mg-8Li-0.5La, (c) Mg-8Li-1La.

3.6 Electrochemical impedance spectra (EIS)

Electrochemical impedance testing techniques are used to further investigate the corrosion and discharge behaviors of the alloy electrodes. Nyquist diagram and Bode plots are shown in Figure 6.

The electrochemical impedance spectra of Mg-8Li, Mg-8Li-0.5La and Mg-8Li-1La electrodes are obtained after immersing the samples in 0.7 mol·L^{-1} NaCl solution for 5 minutes to provide the corrosion and discharge information in the initial stage. According to the Nyquist diagrams, as shown in Figure 6(a), the Nyquist results of Mg-8Li, Mg-8Li-0.5La and Mg-8Li-1La electrodes have one semicircular arc at high frequency. The high-frequency loop is due to the charge transfer process of the double layer at the electrode/electrolyte interface, so the charge transfer resistance determines the size of the semicircular arc corresponding to the electrochemical reaction process[23]. The larger the charge transfer resistance, the greater the hindrance between the electrolyte solution and the electrode surface, and the more difficult the reaction. The Nyquist sizes of Mg-8Li-1La and Mg-8Li-0.5La electrodes over the entire frequency range are larger than that of Mg-8Li electrode, indicating that Mg-8Li-1La and Mg-8Li-0.5La electrodes have better corrosion resistance than Mg-8Li electrode. However, the above results are inconsistent with the corrosion potential results on the polarization curves. Therefore, as suggested by Song et al[15], the corrosion rate of magnesium or magnesium alloy cannot be evaluated simply by the polarization curve. The Bode plots associated with the phase angle and impedance modulus are given in Figure 6(b) and Figure 6(c), respectively. Three samples all exhibit a large phase angle peak connected with the charge transfer process at around 10^2 Hz, and the Mg-8Li electrode possesses the smallest peak among three samples. The deviation of $|Z|$ is the value between the lowest frequency and the highest frequency, which represents the polarization resistance associated with the activity of the electrode system [26]. In contrast, the corrosion resistances of Mg-8Li-0.5La and Mg-8Li-1La electrodes are stronger at the initial stage, as analyzed above, the Mg-8Li-1La electrode exhibits the best suitable activation behavior and corrosion resistance in three samples.

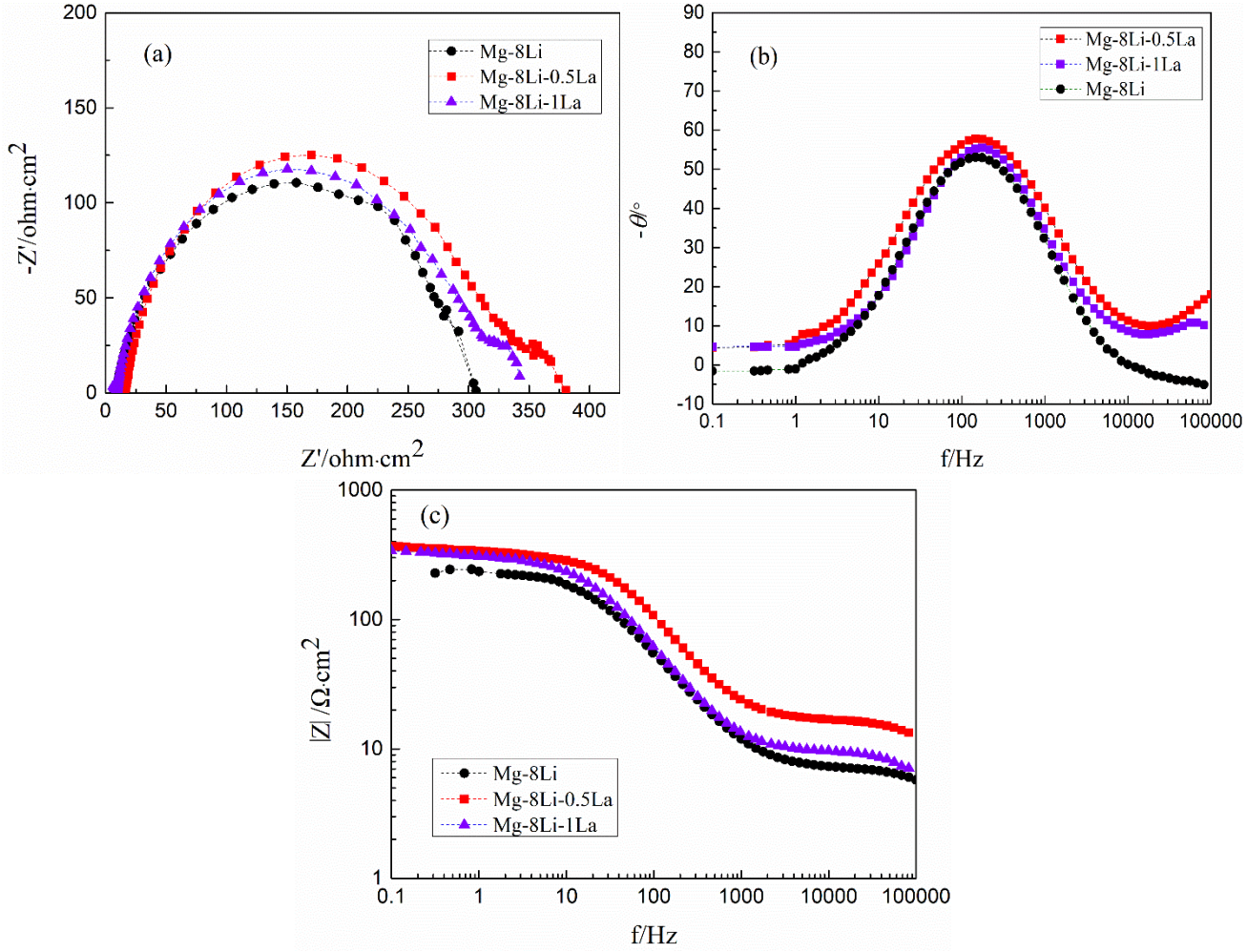

Figure 6. EIS results of Mg-8Li, Mg-8Li-0.5La, and Mg-8Li-1La electrodes in 0.7 mol·L^{-1} NaCl solution, (a) Nyquist plots, (b) Bode plots of phase angle vs. frequency, and (c) Bode plots of impedance modulus vs. frequency.

EIS plots for Mg-8Li, Mg-8Li-0.5La and Mg-8Li-1La electrodes can be fitted through the equivalent circuit shown in Figure 7. In the equivalent circuit, R_s and R_t are the solution resistance and the charge transfer resistance, respectively [16]. Due to the dispersion effect caused by the nonideal plane structure, the ideal capacitance characteristic of the double layer is offset, thus CPE_{dl} is adopted to substitute the capacitance of the double layer. These elements are described by two parameters, i.e., CPE_{dl} and n. The dimension of CPE_{dl} is $\Omega^{-1}\cdot cm^{-2}\ s^n$, and n is an exponent without dimension. The EIS fitting results are listed in Table 5. It can be observed that the Mg-8Li electrode exhibits the smallest values of both R_s and R_t, followed by the Mg-8Li-1La electrode, while both are smaller than the Mg-8Li-0.5La electrode. This phenomenon partially explains that the corrosion resistance of the Mg-8Li electrode is inferior to those of the electrodes containing the element of La. When the electrode surface is not subjected to discharge and is not damaged, the corrosion resistances of Mg-8Li-0.5La and Mg-8Li-1La electrodes are superior to that of the Mg-8Li electrode. The Mg-8Li-1La electrode has a moderately-sized resistance, indicating that the Mg-8Li-1La electrode is stable at the OCP, as confirmed by the corrosion current densities and self-corrosion rates listed in Table 2 and Table 3. The Mg-8Li-1La

electrode with a proper R_t can inhibit the self-corrosion at the OCP and provide a negative potential in the course of discharge.

Table 5. EIS fitting results of Mg-8Li, Mg-8Li-0.5La, and Mg-8Li-1La electrodes.

Alloy electrodes	R_s/(Ω·cm^2)	CPE_{dl}/(Ω^{-1}·cm^{-2}·s^n)	n	R_t/(Ω·cm^{-2})
Mg-8Li	8	7.066×10^{-5}	0.82	294
Mg-8Li-0.5La	13	2.451×10^{-5}	0.94	350
Mg-8Li-1La	10	6.269×10^{-5}	0.86	309

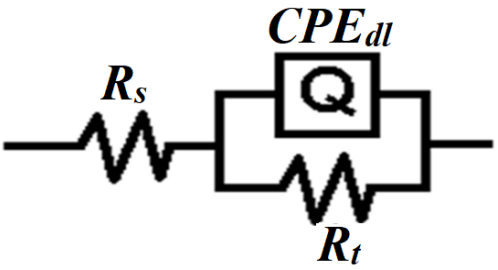

Figure 7. EIS equivalent circuits of Mg-8Li, Mg-8Li-0.5La and Mg-8Li-1La alloy electrodes.

4. CONCLUSIONS

Mg-8Li-1La, Mg-8Li-0.5La and Mg-8Li alloy electrodes were prepared by the melting method, and their electrochemical properties in 0.7 mol·L^{-1} NaCl solution were studied. From the electrochemical measurements and the microstructure characterizations, the following conclusions can be drawn:

1. The Mg-8Li-1La electrode has higher electrochemical activity compared with the Mg-8Li-0.5La electrode and the Mg-8Li electrode;

2. The Mg-8Li-1La alloy has the smallest self-corrosion rate and self-discharge rate. In addition, the Nyquist pattern sizes of Mg-8Li-1La and Mg-8Li-0.5La alloy electrodes are larger than that of the Mg-8Li alloy electrode. The above two aspects illustrate that the addition of La element increases the corrosion resistance of the alloys in static state;

3. The content of La in the Mg-8Li alloy obviously affected the performance of the alloys, and the La content of 1.0% is better than 0.5%.

CONFLICTS OF INTEREST
There are no conflicts to declare.

ACKNOWLEDGMENTS
This work was financially supported by the National College Students' Innovation and Entrepreneurship Training Program Project (No. 201810217163), Natural Science Foundation of Zhejiang Province (No. LY19E010005), No. 6141B042869**,** Key Laboratory Fund Project (No. 6142901180201), and the Natural Science Foundation of Hei-longjiang Province of China under Grant No.LH2020E065.

References

1. R. R. Bessette, M. G. Medeirosa, C. J. Patrissi, C. M. Deschenes, C. N. L. Fratta, *J. Power Sources,* 96 (2001) 240-244.
2. é. Hasvold and N. Stùrkersen, *J. Power Sources,* 96 (2001) 252-258.
3. K. Agbossou, R. Chahine, J. Hamelin, F. Laurencelle, A. Anouar, J. M. St-Arnaud and T.K. Bose, *J. Power Sources,* 96 (2001) 168-172.
4. F. Y. Cheng and J. Chen, *Chem. Soc. Rev.,* 41 (2012) 2172-2192.
5. K. C. Hong, *J. Power Sources,* 96 (2001) 85-89.
6. K. N. Mahesh, R. Balaji and K. S. Dhathathreyan, *Ionics,* 21 (2015) 2603-2607.
7. M. G. Medeiros, R. R. Bessette, C. M. Deschenes, C. J. Patrissi, L. G. Carreiro, S. P. Tucker, and D. W. Atwate, *J. Power Sources,* 136 (2004) 226-231.
8. R. R. Bessette, M. G. Medeirosa, C. J. Patrissi, C. M. Deschenes and C. N. L. Fratta, *J. Power Sources,* 96 (2001) 240-244.
9. Y. Z. Lv, M. Liu, Y. Xu, D. X. Cao and J. Feng, *J. Power Sources,* 225 (2013) 124-128.
10. M. G. Medeirosa, R. R. Bessette, C. M. Deschenesc, and D. W. Atwatera, *J. Power Sources,* 96 (2001) 236-239.
11. N. G. Wang, R. C. Wang, C. Q. Peng, B. Peng, Y. Feng, Y and C. W. Hu, *Electrochim. Acta,* 149 (2014) 193-205.
12. D. X. Cao, L. Wu, Y. Sun, G. L. Wang and Y. Z. Lv, *J. Power Sources,* 177 (2008) 624-630.
13. D. X. Cao, L. Wu, G. L. Wang and Y. Z. Lv, *J. Power Sources,* 183 (2008) 799-804.
14. L. R. Chang, F. H. Cao, J. S. Cai, W. J. Liu, Z. Zhang and J. Q. Zhang, *T. NONFERR. METAL. SOC.,* 21 (2011) 307-316.
15. Y. W. Song, D. Y. Shan, R. S. Chen and E. H. Han, *Corros. Sci.,* 51 (2009) 1087-1094.
16. Y. B. Ma, N. Li, D. Y. Li, M. L. Zhang and X. M. Huang, *J. Power Sources,* 196 (2011) 2346-2350.
17. Y. Z. Lv, Y. Xu and D. X. Cao, *J. Power Sources,* 196 (2011) 8809-8814.
18. Y. Z. Lv, M. Liu, Y. Xu, D. X. Cao, J. Feng, R. Z. Wu and M. Zhang, *J. Power Sources,* 239 (2013) 265-268.
19. Y. Z. Lv, L. L. Bao, F. Meng and X. Gao, *IONICS,* 24 (2018) 1715-1720.
20. Y. Z. Lv, Y. F. Li, L. Wang, D. X. Cao, G. L. Wang, J. Feng, Y. M. Ren and M. L. Zhang, *RSC. Adv.,* 4 (2014) 27236-27241.
21. Y. Z. Lv, L. Wang, Y. F. Li, Y. Z. Jin, J. Feng, Y. M. Ren, D. X. Cao, G. L. Wang and M. L. Zhang, *IONICS,* 20 (2014) 1573-1578.
22. S. Johnston,Z. M. Shi and A. Atrens, *Corros. Sci.,* 101 (2015) 182-192.
23. J. R. Li, Q. T. Jiang, H. Y. Sun and Y. T. Li, *Corros. Sci.,* 111 (2016) 288-301.
24. N. G. Wang, R. C. Wang, C. Q. Peng and Y. Feng, *Corros. Sci,* 81 (2014) 85-95.
25. J. P. Zhang, Y. C. Wang, Y. Feng and C. Q. Peng, *T. NONFERR. METAL. SOC.,* 22 (2012) 3039-3045.
26. N. G. Wang, R. C. Wang, Y. Feng, W. H. Xiong, J. H. Zhang and M. Deng, *Corros. Sci.,* 112 (2016) 13-24.